Proc. SPIE 9033, Medical Imaging 2014: Physics of Medical Imaging, 903313, 2014

Evaluation of low contrast detectability after scatter correction in digital breast tomosynthesis.

Koen Michielsen[a,b] *, Andreas Fieselmann[c], Lesley Cockmartin[b,d], Johan Nuyts[a,b]

[a]Department of Imaging and Pathology, division of Nuclear Medicine & Molecular Imaging, KU Leuven, Leuven, Belgium
[b]Medical Imaging Research Center, KU Leuven, Leuven, Belgium
[c]Siemens Healthcare, Erlangen, Germany
[d]Department of Imaging and Pathology, division of Medical Physics & Quality Assessment, KU Leuven, Leuven, Belgium

ABSTRACT

Projection images from digital breast tomosynthesis acquisitions can contain a large fraction of scattered x-rays due to the absence of an anti-scatter grid in front of the detector. In order to produce quantitative results, this should be accounted for in reconstruction algorithms. We examine the possible improvement in signal difference to noise ratio (SDNR) for low contrast spherical densities when applying a scatter correction algorithm.

Hybrid patient data were created by combining real patient data with attenuation profiles of spherical masses acquired with matching exposure settings. Scatter in these cases was estimated using Monte-Carlo based scattering kernels. All cases were reconstructed using filtered backprojection (FBP) with and without beam hardening correction and two maximum likelihood methods for transmission tomography, with and without quadratic smoothing prior (MAPTR and MLTR). For all methods, images were reconstructed without scatter correction, and with scatter precorrection, and for the iterative methods also with an adjusted update step obtained by including scatter in the physics model. SDNR of the inserted spheres was calculated by subtracting the reconstructions with and without inserted template to measure the signal difference, while noise was measured in the image containing the template.

SDNR was significantly improved by 3.5% to 4.5% ($p < 0.0001$) at iteration 10 for both correction methods applied to the MLTR and MAPTR reconstructions. For MLTR these differences disappeared by iteration 100. For regular FBP SDNR remained the same after correction ($p = 0.60$) while it dropped slightly for FBP with beam hardening correction (-1.4%, $p = 0.028$).

These results indicate that for the iterative methods, application of a scatter correction algorithm has very little effect on the SDNR, it only causes a slight decrease in convergence speed, which is similar for precorrection and correction incorporated in the update step. The FBP results were unchanged because the scatter being corrected is a low frequency component in the projection images, and this information is mostly ignored in the reconstruction due to the high pass filter.

1. INTRODUCTION

Digital breast tomosynthesis (DBT) is an imaging modality using limited angle tomography to reconstruct thick slices. It is usually implemented as an extension of a regular mammography system, using a partially rotating x-ray tube and a stationary detector. Since the anti-scatter grid in the regular mammography system is focused, it cannot be used in tomosynthesis mode, and thus these projections can contain a significant amount of scatter.

Numerous algorithms have been suggested to mitigate the effect of scattered radiation in x-ray imaging. Rührnschopf[1,2] classifies them into deterministic and statistical methods in the projection domain, iterative algorithms that are applied during image reconstruction and image post-processing methods. In general these

*koen.michielsen@uzleuven.be
This work is supported by Siemens Healthcare. Breast tomosynthesis with Siemens MAMMOMAT Inspiration is an investigational practice and is limited by U.S. law to investigational use. It is not commercially available in the U.S. and its future availability cannot be ensured. The concepts and information presented in this paper are based on research and are not commercially available.

algorithms produce more quantitative reconstructions, while the effect on image quality seems to be more varied.[3–5] Specifically for DBT, Liu[3] found no improvement in SDNR and number of detected image feature targets in a physical phantom when using scatter correction for filtered backprojection (FBP), backprojection (BP) or a proprietary FBP implementation. On the other hand, Feng[4] did find that correcting for scatter increased SDNR of low contrast lesions in the CIRS 082 phantom, and improved visualization of lesions in patient cases when using maximum likelihood-expectation maximization (MLEM) reconstruction. A second iterative method, the simultaneous algebraic reconstruction technique (SART), was also found to improve SDNR in simulated phantom images by Wu,[5] but these results can not be directly compared to those of Lui or Feng since scatter was removed physically by a grid, which also removes the additional noise introduced by the scatter, something which is not possible when using a post-acquisition digital scatter reduction method.

In this study we will investigate the effect of scatter correction on low contrast detectability in DBT, described by signal difference to noise ratio by using real patient data with inserted spherical masses, and this for several reconstruction methods.

2. MATERIALS AND METHODS

We evaluate the effect of scatter correction on SDNR of inserted low contrast spherical densities in real patient data for different reconstruction methods. In this section we describe the creation of hybrid projection images, scatter estimation, image reconstruction and analysis methods.

2.1 Creating Hybrid Projections Images

Cockmartin et al[6] proposed a technical-clinical method to create attenuation templates of clinically relevant objects, based on the ratio of projections of these objects and the projections of their homogeneous background, for later insertion in patient images. Spheres made of breast tissue simulating material (CIRS, Norfolk VA, USA) and with a diameter of 5 mm were used to represent mass lesions. Three different densities were used, namely 0%, 30% and 50% breast density equivalence. To adequately simulate the surrounding adipose tissue in the breast, the spheres were submersed in vegetable oil. The height of the oil was varied in order to represent a range of compressed breast thicknesses (i.e. 45 mm of oil was used to represent breasts between 40 and 50 mm).

High dose acquisitions with beam qualities as in patient image acquisitions were performed with and without the spheres present in the oil bath on our clinical breast tomosynthesis system (MAMMOMAT Inspiration; Siemens AG, Healthcare Sector, Erlangen, Germany). The tube current-time product (mAs) was set as high as possible (500 mAs) and each image was acquired five times and then averaged into one image. This avoids additional noise in the hybrid patient images after insertion of the templates. The templates were then created based on simple image division of the images with and without the sphere present in the oil bath. Next, the spheres were manually segmented and normalized by the average background signal, measured in four regions of interest in the homogeneous oil closely around the spheres. This normalization was performed to eliminate short term reproducibility errors, which can arise due to small instabilities in the image acquisition process. These templates, which now capture the properties of the imaging system, were multiplied into unprocessed DBT projection images of patients with corresponding equivalent breast thicknesses in order to obtain hybrid images of spherical densities within anatomical backgrounds.

In this study we selected 57 patient cases with compressed breast thickness between 30 and 79 mm. All acquisitions were used to generate cases which include the lowest density simulated lesion (0%). Cases with thickness between 60 and 69 mm were used to create versions which included densities with contrast of 30% breast density equivalence. The selection is summarized in table 1.

2.2 Scatter Estimation

For scatter estimation, we use a deterministic method in the projection domain based on scattering kernels.[7,8] This method can be implemented such that it is computationally fast. Scattering kernels were computed by Monte-Carlo simulations using polychromatic x-ray spectra and the geometry from a breast tomosynthesis system (MAMMOMAT Inspiration) and different kinds of breast tissue models. Oblique incidence of the X-ray from non-zero projection angles was accounted for by a correction factor similar to the work by Wu et al.[5]

Thickness	Number of cases	Lesion density
30 – 39 mm	10	0%
40 – 49 mm	13	0%
50 – 59 mm	11	0%
60 – 69 mm	12	0%, 30%
70 – 79 mm	11	0%

Table 1. Overview of patient cases.

Using this estimation method, precorrected projection data were created by subtracting the scatter estimate from the original projection data. This resulted in four sets of projection data for each patient case: with and without an inserted sphere and with and without scatter correction.

2.3 Image Reconstruction

The projection data (without scatter correction and with scatter precorrection) were reconstructed using two iterative methods and one filtered backprojection method. The uncorrected data were reconstructed with two further iterative methods that include scatter in the acquisition model of the algorithm. The iterative methods are based on a Poisson model of the image acquisition. Although this noise model is no longer valid after the scatter correction, we assume it is still a reasonable approximation because the correction is very smooth within the projected area of the breast, resulting in relatively homogeneous changes to the noise. The Poisson model produces log-likelihood $L = \sum_i y_i \ln \hat{y}_i - \hat{y}_i$, with measured data y_i, and acquisition model $\hat{y}_i$ which includes intersection lengths l_{ij}, blank scan b_i, and attenuation distribution $\vec{\mu}$, as shown in equation 1. The acquisition model can also include an additive scatter factor s_i, as in equation 2.

$$\hat{y}_i = b_i e^{-\sum_j l_{ij}\mu_j} \tag{1}$$

$$\hat{y}_i = b_i e^{-\sum_j l_{ij}\mu_j} + s_i \tag{2}$$

Log-likelihood L is maximized in order to obtain the measured attenuation distribution $\vec{\mu}$. The optimization is done using the Maximum Likelihood for Transmission (MLTR) algorithm,[9] which provides the additive iteration scheme in equation 3, with $\Delta\mu_j$ dependent on the acquisition model. The Maximum a Posteriori for Transmission (MAPTR) update steps, which include a smoothing prior P with strength β are shown in equation 4 for the acquisition model without scatter, and equation 5 for the acquisition model with scatter. Choosing $\beta = 0$ results in the update equation for the original MLTR form. Reconstructions were stopped after 100 iterations.

$$\mu_j^{n+1} = \mu_j^n + \Delta\mu_j^n \tag{3}$$

$$\Delta\mu_j = \frac{\sum_i l_{ij}\left(\hat{y}_i - y_i\right) + \beta \sum_k w_{jk} \frac{\partial P(\mu_j,\mu_k)}{\partial \mu_j}}{\sum_i l_{ij}\left(\sum_h l_{ih}\right)\hat{y}_i - 2\beta \sum_k w_{jk} \frac{\partial^2 P(\mu_j,\mu_k)}{\partial \mu_j^2}} \tag{4}$$

$$\Delta\mu_j = \frac{\sum_i l_{ij}\left(\hat{y}_i - y_i\right)\frac{\hat{y}_i - s_i}{\hat{y}_i} + \beta \sum_k w_{jk} \frac{\partial P(\mu_j,\mu_k)}{\partial \mu_j}}{\sum_i l_{ij}\left(\sum_h l_{ih}\right)\frac{\left(\hat{y}_i - s_i\right)^2}{\hat{y}_i} - 2\beta \sum_k w_{jk} \frac{\partial^2 P(\mu_j,\mu_k)}{\partial \mu_j^2}} \tag{5}$$

$$P\left(\mu_j, \mu_k\right) = -\left(\mu_j - \mu_k\right)^2 \tag{6}$$

In the MAPTR reconstruction without scatter correction $\beta = 10^5$ was chosen. The value of β needs to be adjusted for the reconstructions with precorrection and with the modified algorithm in equation 5 to make sure the smoothing prior has the same strength relative to the likelihood term in the numerator. When using the update step in formula 4 with a precorrection, the likelihood term doesn't change since scatter is subtracted from

both $\hat{y}_i$ and y_i. The prior term does increase in strength since it depends on the quadratic difference between attenuation values, which change due to the scatter correction. In practice, attenuation values increased by 20%, increasing the weight of the prior term by 44%. To compensate β was set to $0.7 \cdot 10^5$. For the modified update step, the likelihood term is changed with a factor $(\hat{y}_i - s_i)/\hat{y}_i$ which can be approximated by $1 - \mathrm{SF}$ with SF the scatter fraction in the projection images. The resulting β is then $(1 - \mathrm{SF}) \cdot 0.7 \cdot 10^5$. The scatter fraction used for this calculation was derived from a linear fit to the measured scatter fraction behind the breast for all projection images in all patient cases, as shown in figure 1.

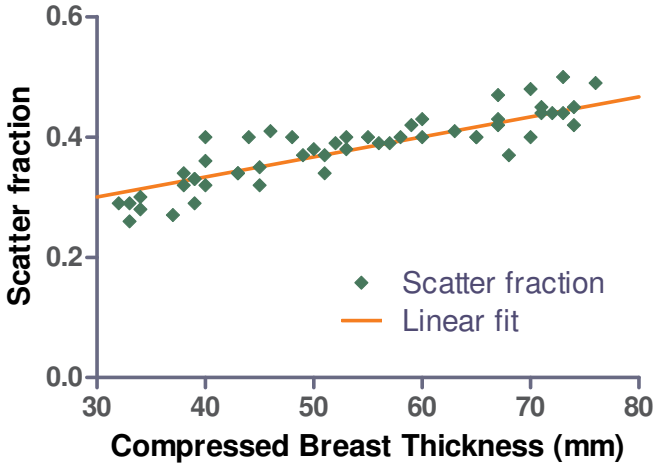

Figure 1. Scatter fraction in all patient cases, with linear fit.

The FBP method is adapted to the limited angle cone beam geometry, similar to an FDK[10] type algorithm. It includes a filtering step which performs an approximate inversion of the system modulation transfer function (MTF), a spectral filter and a slice thickness filter.[11] A variant of this method applies a beam hardening correction (BHC) on the projection data before the filtering step.

2.4 Data Analysis

After reconstruction, matching cases with and without inserted mass were subtracted in order to obtain an image which contains only the signal difference. The SDNR is then calculated by dividing the mean pixel value inside the lesion in the subtracted image by the root mean square of the standard deviations inside a series of half-overlapping 8×8 pixel regions in the location of the lesion, in the image containing the lesion. The mean signal, standard deviation and SDNR are calculated for each dataset and select comparisons are made between all reconstructions at iterations 10 and 100 using using a repeated measures ANOVA analysis followed by Tukey's post test to compare results from both correction methods to the uncorrected reconstruction. The FBP reconstructions with and without scatter correction were compared using a two sided paired t-test.

Comparisons where made at iteration 100 because here reconstructions were approaching convergence while reconstruction time remained feasible for the large datasets. An additional comparison was made at iteration 10 because reconstructions of preliminary experiments with calcifications with a diameter of 250 μm showed peak SDNR roughly around iteration 10, as shown in figures 2 and 3 for patient with compressed breast thickness in the range of 30 to 39 mm and 60 to 69 mm.

3. RESULTS

Figure 4 shows an example of the region around the inserted sphere for a MAPTR reconstruction with and without scatter precorrection. Figures 5 and 6 show SDNR of the 0% and 30% density contrast spheres as a function of the number of iterations. The results from the reconstructions using the modified update step in equation 5 are not shown since they overlap with the results of the reconstruction with precorrection. The result of the FBP reconstructions is shown as a horizontal line in the graph. This line represents both FBP methods with and without scatter correction because they produced overlapping data. It crosses the iterative results

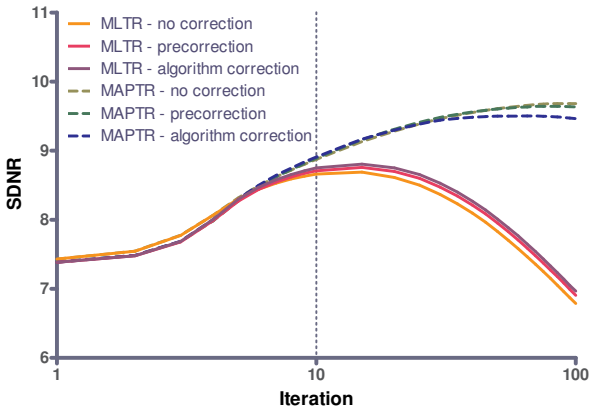

Figure 2. Average SDNR values for calcifications with a diameter of 250 μm in a 30 mm breast.

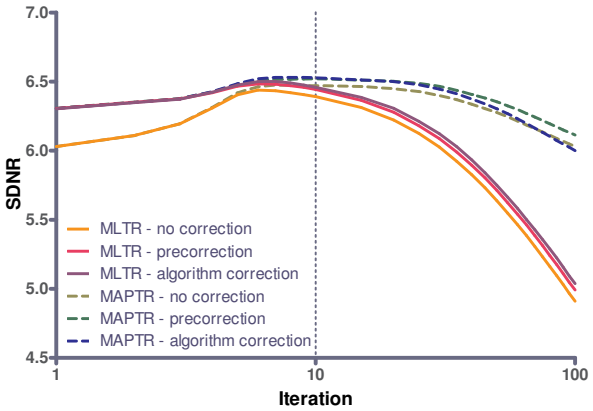

Figure 3. Average SDNR values for calcifications with a diameter of 250 μm in a 60 mm breast.

between iterations 15 and 20 for both graphs. Figure 7 plots the SDNR values of the 0% density contrast sphere at the tenth iteration as a function of compressed breast thickness, with the same overlapping data left out as in the previous graphs.

Statistical test results of the ANOVA analysis with Tukey's post test for the differences in SDNR values at iterations 10 and 100 of the 0% density contrast sphere are listed in table 2. Critical q-values for the post test are 3.34 for a 95% confidence interval, and 4.18 for a 99% confidence interval.

Table 3 lists signal, noise and SDNR for the patient cases with compressed breast thickness between 60 and 69 mm. The statistical test results for these data can be found in table 4. Critical q-values for the post test are 3.47 for a 95% confidence interval, and 4.41 for a 99% confidence interval.

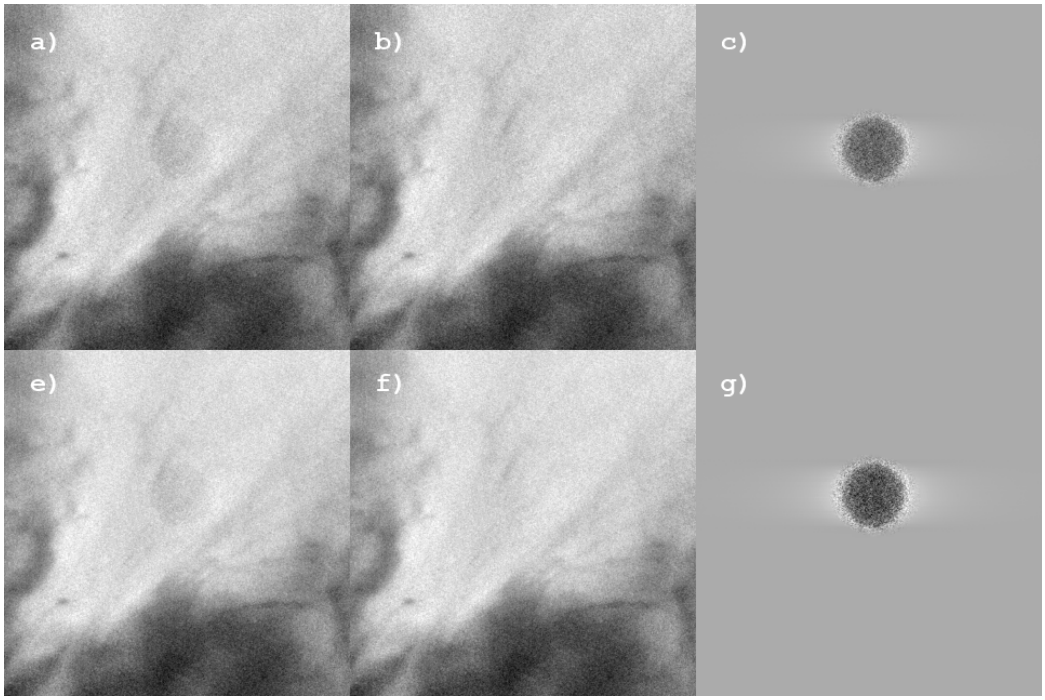

Figure 4. MAPTR reconstruction for one case, with all subfigures rescaled to the same minimum and maximum. a) without scatter correction, with density; b) without scatter correction, without density; c) difference between a) and b); e) with scatter precorrection, with density; f) with scatter precorrection, without density; g) difference between e) and f).

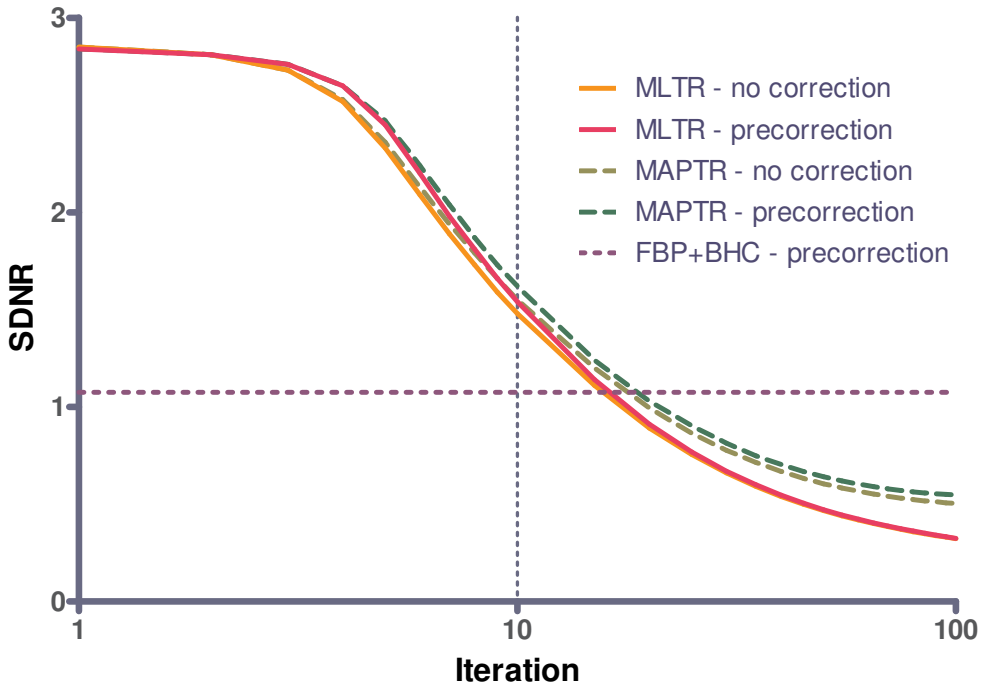

Figure 5. SDNR of the 0% density sphere for patients with compressed breast thickness between 60 and 69 mm.

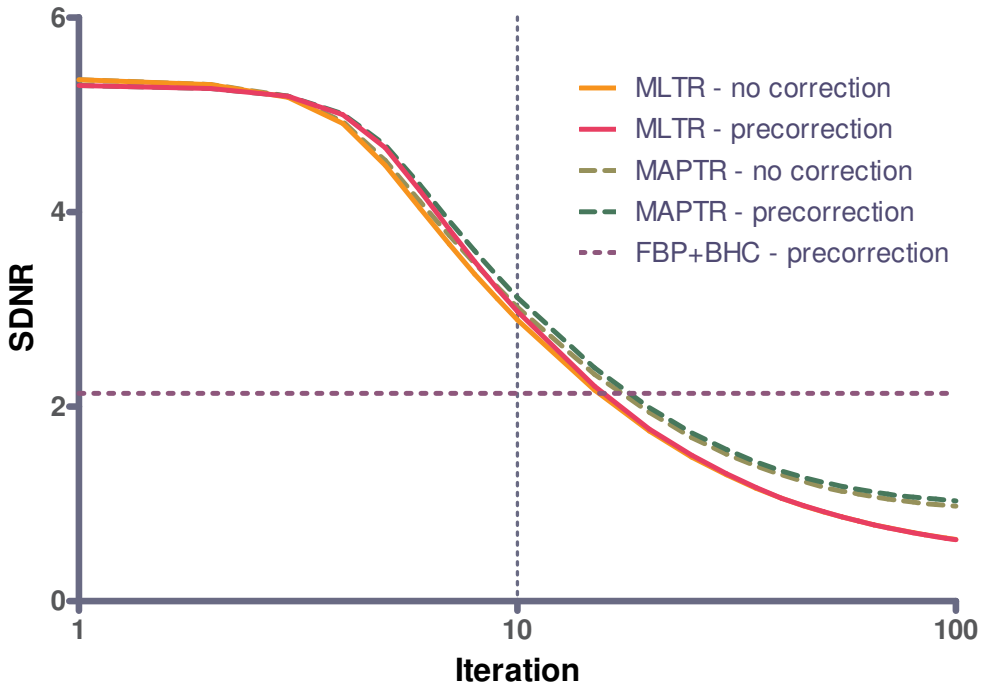

Figure 6. SDNR of the 30% density sphere for patients with compressed breast thickness between 60 and 69 mm.

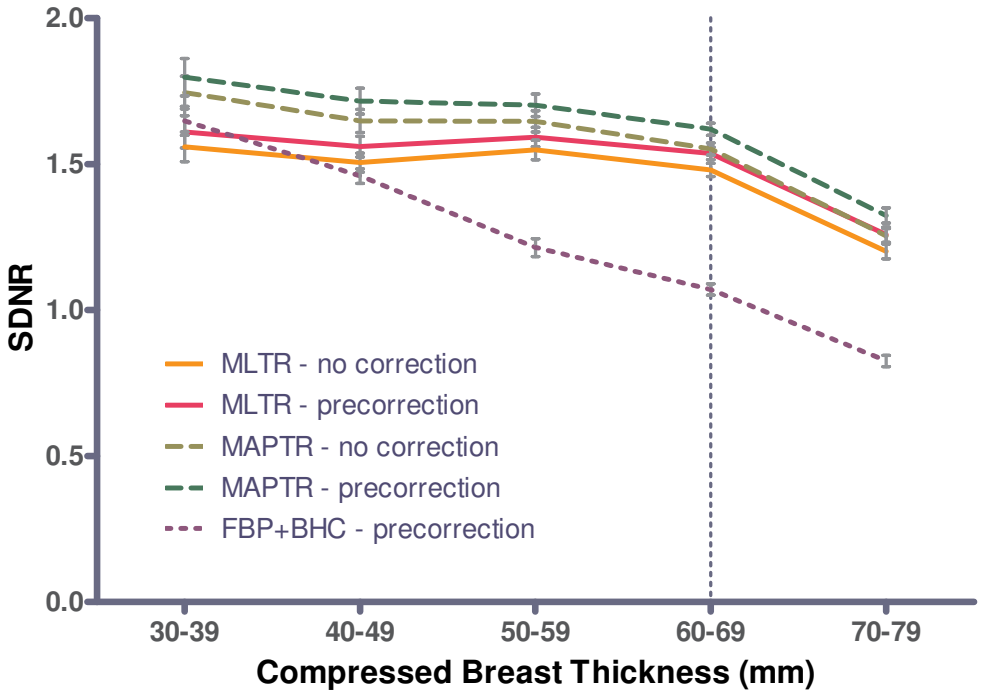

Figure 7. SDNR of the 0% density sphere at the tenth iteration for all compressed breast thickness groups.

Reconstruction	Precorrection			Algorithm change		
	SDNR change	p-value	q-value	SDNR change	p-value	q-value
MLTR (10it)	+3.6%	<0.0001	26.63	+3.5%	<0.0001	25.74
MLTR (100it)	+0.5%	<0.0001	**3.097**	-0.6%	<0.0001	3.918
MAPTR (10it)	+4.0%	<0.0001	19.90	+4.0%	<0.0001	19.98
MAPTR (100it)	+6.5%	<0.0001	8.918	+7.2%	<0.0001	9.983
FBP	+0.2%	**0.101**				
FBP + BHC	-0.2%	**0.517**				

Table 2. Differences, p-values, and q-values for comparing both scatter correction methods to the baseline without scatter correction, for the 0% density contrast sphere in all thickness groups combined. Critical q-values for the post test are 3.34 for a 95% confidence interval, and 4.18 for a 99% confidence interval. Non-significant p- and q-values are printed in bold.

Reconstruction	No scatter correction			Precorrection			Algorithm change		
	Signal	Noise	SDNR	Signal	Noise	SDNR	Signal	Noise	SDNR
MLTR (10it)	.000 976	.000 662	1.48	.001 623	.001 062	1.54	.001 617	.001 060	1.53
MLTR (100it)	.001 429	.004 449	0.32	.002 511	.007 792	0.33	.002 474	.007 784	0.32
MAPTR (10it)	.000 963	.000 623	1.55	.001 594	.000 987	1.62	.001 589	.000 984	1.62
MAPTR (100it)	.001 426	.002 831	0.50	.002 498	.004 537	0.55	.002 463	.004 474	0.55
FBP	162.3	151.7	1.07	214.9	201.2	1.07			
FBP + BHC	232.6	214.8	1.09	298.5	279.6	1.07			

Table 3. Mean signal, mean noise and mean SDNR values of the 0% density sphere for patients with compressed breast thickness between 60 and 69 mm.

Reconstruction	Precorrection			Algorithm change		
	SDNR change	p-value	q-value	SDNR change	p-value	q-value
MLTR (10it)	+3.7%	<0.0001	23.99	+3.5%	<0.0001	22.86
MLTR (100it)	+0.3%	0.007	3.637	-1.0%	0.007	**2.763**
MAPTR (10it)	+4.5%	<0.0001	13.94	+4.5%	<0.0001	13.54
MAPTR (100it)	+9.3%	0.0011	5.280	+9.3%	0.0011	5.392
FBP	-0.2%	**0.60**				
FBP + BHC	-1.4%	0.028				

Table 4. Differences, p-values, and q-values for comparing both scatter correction methods to the baseline without scatter correction, for all 0% density cases with compressed breast thickness between 60 and 69 mm. Critical q-values for the post test are 3.47 for a 95% confidence interval, and 4.41 for a 99% confidence interval. Non-significant p- and q-values are printed in bold.

4. DISCUSSION

The first conclusion is that the effect of scatter correction in the iterative methods is mainly a change in convergence speed, as can be seen in the MLTR curves in figures 5 and 6. The differences in SDNR between the methods at iteration 10 almost disappear by iteration 100. Table 4 shows that a difference remains for the precorrection, but this is small and only just significant. When combining all thickness groups as in table 2, it is the difference between the uncorrected reconstruction and the reconstruction with modified update step that is significant, but again only just and with small actual difference. We suspect these remaining differences are the result of differences in convergence speed.

A larger difference remains between the SDNR of the corrected and uncorrected MAPTR reconstruction, both for the 60 to 69 mm group and for all data combined, but it is not clear whether this is caused by a true difference, by an incorrect modification of the β parameter applied to ensure the relative strength of likelihood and prior were the same for all reconstruction, or by convergence differences between the MAPTR reconstructions after 100 iterations.

As shown in figure 7, the difference in SDNR between methods remains constant for different thickness groups. The SDNR of the iterative methods are less influenced by thickness than the FBP reconstructions.

No effect of scatter correction on the SDNR of the FBP images was observed. This is probably because the scatter being corrected is a low frequency component in the projection images, and this information is mostly ignored in the reconstruction due to the high pass filter. The combination of a beam hardening correction and a scatter correction shows a small negative trend, which might be caused by the fact that the applied beam hardening correction is currently tuned for data that includes scatter and should be adapted for use on scatter corrected data.

5. CONCLUSIONS

Our results indicate that applying a scatter correction method only has an effect on lesion SDNR in iterative reconstructions due to a small change in convergence speed. The fact that there is barely a difference in the results of both scatter correction methods, allows us to choose the simpler precorrection method when it is necessary to obtain quantitative reconstructed data.

REFERENCES

[1] Rührnschopf, E.-P. and Klingenbeck, K., "A general framework and review of scatter correction methods in x-ray cone-beam computerized tomography. Part 1: Scatter compensation approaches," *Medical Physics* **38**(7), 4296–4311 (2011).

[2] Rührnschopf, E.-P. and Klingenbeck, K., "A general framework and review of scatter correction methods in cone beam CT. Part 2: Scatter estimation approaches," *Medical Physics* **38**(9), 5186–5199 (2011).

[3] Liu, B. and Li, X., "Effects of scatter radiation on reconstructed images in digital breast tomosynthesis," in [*SPIE Medical Imaging: Physics of Medical Imaging*], Samei, E. and Hsieh, J., eds., *SPIE Proceedings* **7258**, 72585Y, SPIE (Feb. 2009).

[4] Feng, S. S. J. and Sechopoulos, I., "A software-based x-ray scatter correction method for breast tomosynthesis," *Medical Physics* **38**(12), 6643–6653 (2011).

[5] Wu, G., Mainprize, J. G., Boone, J. M., and Yaffe, M. J., "Evaluation of scatter effects on image quality for breast tomosynthesis," *Medical Physics* **36**(10), 4425–4432 (2009).

[6] Cockmartin, L., Stalmans, D., Zanca, F., Marshall, N. W., Dance, D. R., Young, K. C., Shaheen, E., and Bosmans, H., "A new hybrid technical-clinical test demonstrates improved low contrast detectability in tomosynthesis when compared to 2D mammography," *presented at RSNA* (2012).

[7] Sechopoulos, I., Suryanarayanan, S., Vedantham, S., D'Orsi, C. J., and Karellas, A., "Scatter radiation in digital tomosynthesis of the breast," *Medical Physics* **34**(2), 564–576 (2007).

[8] Díaz, O., Dance, D. R., Young, K. C., Elangovan, P., Bakic, P. R., and Wells, K., "A fast scatter field estimator for Digital Breast Tomosynthesis," in [*SPIE Medical Imaging: Physics of Medical Imaging*], Pelc, N. J., Nishikawa, R. M., and Whiting, B. R., eds., *SPIE Proceedings* **8313**, 831305, SPIE (Feb. 2012).

[9] Nuyts, J., De Man, B., Dupont, P., Defrise, M., Suetens, P., and Mortelmans, L., "Iterative reconstruction for helical CT: a simulation study.," *Physics in Medicine and Biology* **43**, 729–737 (Apr. 1998).

[10] Feldkamp, L. A., Davis, L. C., and Kress, J. W., "Practical cone-beam algorithm," *Journal of the Optical Society of America A* **1**, 612–619 (June 1984).

[11] Mertelmeier, T., Orman, J., Haerer, W., and Dudam, M. K., "Optimizing filtered backprojection reconstruction for a breast tomosynthesis prototype device," in [*SPIE Medical Imaging: Physics of Medical Imaging*], Flynn, M. J. and Hsieh, J., eds., *SPIE Proceedings* **6142**, 61420F, SPIE (Mar. 2006).